BNL-225754-2024-JAAM

Assembling Vertical Block Copolymer Nanopores via Solvent Vapor Annealing on Homopolymer-Functionalized Substrates

B. Bellini, G. S. Doerk

To be published in "ACS Applied Materials & Interface"

June 2024

Center for Functional Nanomaterials

Brookhaven National Laboratory

U.S. Department of Energy

USDOE Office of Science (SC), Basic Energy Sciences (BES). Scientific User Facilities (SUF)

DISCLAIMER

Assembling Vertical Block Copolymer Nanopores via Solvent Vapor Annealing on Homopolymer-Functionalized Substrates

Beatrice Bellini,[‡†] Jasmine R. Willard,[◊] Semih Cetindag,[†] Esther H. R. Tsai,[†] Ruipeng Li,[⁜] Kim Kisslinger,[†] Sanat K. Kumar,[‡] Gregory S. Doerk[†,]*

[‡] Department of Chemical Engineering, Columbia University, New York, NY 10027, USA.

[†]Center for Functional Nanomaterials, Brookhaven National Laboratory, Upton, New York NY-11973, USA.

◊Alfred University, Alfred, NY 14802, USA

[⁜] National Synchrotron Light Source II, Brookhaven National Laboratory, Upton, NY 11973, USA.

KEYWORDS: Block copolymer self-assembly, nanopatterning, polymer template, high χN system, solvent vapor annealing

ABSTRACT

Utilizing the self-assembly of block copolymers with large Flory-Huggins interaction parameters (χ) for nanofabrication is a formidable challenge due to the attendant large surface energy differences between the blocks. This work reports a robust protocol for the fabrication of thin films with highly-ordered cylindrical nanopore arrays via the self-assembly of an asymmetric poly (styrene-*block*-4-vinyl pyridine) (PS-*b*-P4VP) diblock copolymer blended with P4VP homopolymer. The desired vertical domain orientation is achieved at the air-polymer interface by controlled solvent vapor annealing (SVA) using acetone, a solvent with weak selectivity for PS over P4VP, and at the substrate interface by functionalization using a hydroxy-terminated poly(2-vinylpyridine) (P2VP-OH) homopolymer brush. In contrast, vertical cylinder orientation is unstable during acetone SVA on substrates functionalized using hydroxy-terminated poly(methyl methacrylate) (PMMA-OH). Though PMMA exhibits more balanced interfacial energies between PS and P4VP than P2VP in the dry state, it is also swollen more selectively by acetone. We hypothesize that the nearly balanced solvent swelling of the three polymers (P2VP, P4VP and PS) stabilizes the vertical cylinder orientation, while unbalanced swelling (PMMA > P4VP and PS) does not. We further characterize pore formation by addition of P4VP homopolymer and its post-assembly extraction using ethanol, revealing a narrow window of pore size tunability. Notably, minimal differences in nanopore morphologies are observed for P4VP volume fractions as high as 0.1, regardless of the P4VP molar mass. However, further increasing the P4VP volume fraction results in domain reorientation or macrophase separation when its molar mass is less than or greater than the P4VP block molar mass, respectively. Using a P4VP homopolymer that is nearly equal in length with the P4VP block enables fabrication of well-ordered arrays of vertical, through-film nanopores with high aspect ratios (> 10), small periods (< 23 nm) and diameters less than 10 nm.

INTRODUCTION:

High-aspect ratio vertical nanopore arrays synthesized through the spontaneous self-assembly of block copolymer (BCP) thin films have attracted intense interest for applications in nanolithography,[1–3] membrane separations,[4–6] Li battery anode protection,[7] and templating nanomaterial synthesis.[8] A majority of BCP nanopatterning applications have utilized polystyrene-*block*-poly(methyl methacrylate) (PS-*b*-PMMA) based on the near equal surface energies of the two blocks at elevated temperatures (> 200 °C) at the air-polymer interface. As a result, robust vertical domain orientation is achievable with PS-*b*-PMMA films via simple thermal annealing after first "neutralizing" the supporting substrate surface using a chemically grafted random copolymer “brush” composed of PS and PMMA monomers that balances interfacial energy between the substrate and the PS and PMMA blocks.[9] Indeed, through-film vertical domain orientation for aspect ratios (film thickness/domain period) higher than 13 is possible with judicious selection of brush composition and annealing temperature.[10] A major limitation of PS-*b*-PMMA, however, is its low Flory-Huggins interaction parameter, χ, which prevents domain scaling to the sub-10 nm range.[11] This limit has driven a substantial amount of research in thin film self-assembly of higher χ BCPs;[12] the drawback of such polymer systems is that the chemical dissimilarity between the blocks yields a large χ which is frequently accompanied by a concomitantly large surface energy difference. This surface energy difference renders a selective air interface, thereby frustrating vertical domain orientation.

Solvent vapor annealing (SVA) offers a general approach to circumvent this limitation that is applicable to a wide range of BCPs. In this method, the BCP film is swollen with a solvent that acts as a plasticizer, reducing the system glass transition to below the ambient temperature, thus

mobilizing the BCP to allow domain rearrangement and ordering.[13] SVA using solvents with appropriate selectivity for the blocks can create an effectively balanced free energy top surface that promotes vertical domain orientation,[14–16] in some cases even without substrate surface treatment.[17] However, reported studies frequently use very thin BCP films, thereby yielding low aspect ratio (< ~2) vertical domains. Indeed, as shown by Lee et al. in an investigation of SVA using different solvents for thick asymmetric polystyrene-block-polyisoprene films, while SVA reinforces incipient vertical cylinder orientation at the free interface in as-cast films, cylinders near the selective substrate interface remain horizontal.[18] Eventually a gradual cylinder reorientation propagates throughout the film from the substrate surface. Nonselective (i.e., "neutral") solvents actually promote faster reorientation as a result of enhanced assembly kinetics due to screening of net repulsive block interactions by the solvent (i.e., reduced effective χ).[19]

These results demonstrate that substrate treatment is generally necessary for vertical domain orientation in coil-coil BCP films by SVA, particularly as film thickness is increased. However, surface treatment options for high χ BCPs are limited in comparison to PS-*b*-PMMA. The use of random copolymer brushes discussed previously for PS-*b*-PMMA has been extended to a higher χ BCP, polystyrene-*block*-poly(2-vinyl pyridine),[20] but incompatible polymerization mechanisms prohibit random copolymer synthesis for many other BCP systems.[21] Blending homopolymer brushes that are chemically identical to the two blocks,[22] or sequential brush grafting,[23] can be used for substrate neutralization as well, though these are complicated by the tendency for brush polymer phase separation, a problem that is exacerbated in higher χ systems. In principle, chemically distinct homopolymer brushes may be used to balance interfacial tensions between the blocks and the substrate. Indeed, Pang et al. demonstrated the use of a library of homopolymer brushes and cross-linked "mats" comprising combinations of phenyl and ester

groups for substrate neutralization applicable to PS-*b*-PMMA, poly(styrene-*block*-*rac*-lactide), poly(styrene-*block*-propylene carbonate)[21] and poly(styrene-*block*-methyl acrylate).[24] It is unclear, however, how to generalize the use of homopolymer brushes with these monomer chemistries to other BCPs.[25] Moreover, chemically distinct homopolymer neutral brushes have only been demonstrated for thermally annealed BCP films; their use with SVA is complicated by the addition of solvent, which can swell the brush to a different degree than the BCP blocks, thereby altering the interactions between all the polymers in the system and potentially disrupting the delicate interfacial energy balance which stabilizes vertical domain orientation.

Besides controlling self-assembled domain orientation, the formation of high aspect ratio nanopore arrays hinges on reliable and uniform pore formation methods. Selective block etching[26] or swelling[27,28] are well-established methods but are not available to all BCP chemistries. In contrast, blending of BCPs with homopolymers (HPs) that are solubilized by the minority block and can be extracted by a selective solvent present a compelling general alternative.[16,29,30] Notably, adjusting the HP molar mass or volume fraction presents a means of tuning pore size using a single BCP for customized nanofabrication masks or membrane materials. However, a dearth of reports for BCP/HP blend films assembling to vertical cylinder domains with high aspect ratios (> ~2) makes guidelines for HP selection unclear.

In this work, we report the results of investigations of the self-assembly of thin film blends of an asymmetric poly(styrene-block-4-vinyl pyridine) (PS-*b*-P4VP), a versatile high χ diblock copolymer,[31] and P4VP homopolymer, by SVA on homopolymer-functionalized substrates. Through these investigations, we develop a protocol for the robust fabrication of well-ordered arrays of vertical nanopores with diameters tunable to less than 10 nm and aspect ratios as high as ~10. Our protocol is based on the combination of automated, feedback-controlled SVA with

acetone, a weakly PS-selective solvent, and substrate functionalization with a hydroxy-terminated poly(2-vinylpyridine) (P2VP-OH) homopolymer. The limited stability of vertical cylinders on substrates functionalized using hydroxy-terminated poly(methyl methacrylate) (PMMA-OH), which exhibits more balanced interfacial energies with the blocks than P2VP but swells more selectively with acetone, implies that nonselective swelling of P2VP with respect to PS or P4VP is important for successful vertical cylinder orientation. In addition, the molar mass of the P4VP homopolymer is shown to be especially important for stabilizing vertical orientation with wide pore size tunability, where a larger volume fraction of P4VP homopolymer can be blended with the PS-*b*-P4VP when its molar mass is approximately equal to the P4VP block molar mass. Higher P4VP homopolymer molar mass leads to macrophase separation at lower homopolymer volume fractions, while a lower P4VP homopolymer molar mass induces horizontal cylinder assembly.

1. Experimental Section

1.1. Materials

A PS-*b*-P4VP diblock copolymer (19-*b*-5 kg/mol; PDI=1.06) was used, as were P4VP homopolymers with three different molar masses (3 kg/mol, 6 kg/mol, 12 kg/mol). Hydroxy-terminated PS (PS-OH; M_n = 6.0 kg/mol), hydroxy-terminated PMMA (PMMA-OH; M_n = 6.5 kg/mol), hydroxy-terminated P2VP (P2VP-OH; M_n = 6.2 kg/mol) were grafted to boron-doped polished Si wafers (~500 μm thick, ⟨100⟩ orientation, resistivity range of 0–100 ohm-cm (University Wafers)) surface. Solvent swelling experiments were performed using P2VP, PS, P4VP, and PMMA homopolymers with molar masses equal to 855 kg/mol, 877 kg/mol, 77.5 kg/mol, and 769 kg/mol, respectively. All polymers were obtained from Polymer Source Inc. Tetrahydrofuran (THF), methanol, 2-methoxyethanol, propylene glycol methyl ether acetate (PGMEA), ethanol, and diiodomethane were received from Sigma Aldrich and used without

further purification. Deionized water collected from a Millipore water filtration system (water resistance ~18.2 MΩ) was used to perform the contact angle measurements.

1.2. Surface modification

Solutions containing the hydroxy-terminated polymer "brushes" at concentrations of 1% by weight in PGMEA were prepared and stirred for 24 hours to allow the polymer to dissolve completely in the solvent. Silicon wafer substrates were cleaned by exposure to an oxygen plasma (oxygen pressure = 100 mTorr) in a reactive ion etcher (Nordson March CS-1701 RIE) for 120 s at 21 W to remove carbon contamination. The solutions were spin coated onto the cleaned silicon wafers using a two-step recipe, with an angular velocity of 1500 rpm for 30 s in the first step and 5000 rpm for 5 s in the second step. The second step is performed to remove extra liquid built up in the rectangular corners of the samples and it does not affect the as-spun film thickness. The brush polymers were grafted to the substrates via a dehydration reaction between the hydroxy-terminated polymer end and the hydroxy-terminated substrates. This reaction was induced by baking substrates at 250 °C for 5 min on a hot plate (Apogee 300 Bake Plate) under nitrogen purging; the ungrafted chains were removed through washing with PGMEA on the spin coater at 3000 rpm for 30 s. Grafted brush thicknesses measured by spectroscopic ellipsometry (M-2000U, J. A. Woollam Co. Inc) were 4.7 ± 0.1 nm , 4.1 ± 0.1 nm , and 5.0 ± 0.1 nm for PS-OH, PMMA-OH, and P2VP-OH, respectively. The radii of gyration for polymer brushes used here are all ~2 nm.

1.3. Film Deposition and Pore Formation

The BCP solution of 3% (w/w) PS-*b*-P4VP in THF was prepared and stirred for 24 hours to allow the polymer to dissolve completely in the solvent. Then it was blade coated onto the modified silicon wafer.[32] A typical velocity of 55 mm/s was used to obtain 110-130 nm thick films. Systematic film thickness experiments were conducted using constant acceleration sweeps from

0-100 mm/s to yield polymer film thicknesses in the range of 30-200 nm. P4VP homopolymers with varying molar masses were dissolved in methanol and stirred for 24 hours to obtain 3% (w/w) solutions that were then added to the main BCP solution in prescribed ratios. These solutions were blade coated onto the modified silicon wafer in the same manner as the unblended PS-*b*-P4VP, achieving similar thicknesses. The total P4VP HP volume fractions in the blends that were investigated were 5, 9, 19 and 28 % (v/v). The volume fractions were calculated from mass fractions assuming a density of the P4VP (ρ_{P4VP} = 1.15 g/ml) and a calculated average density of the (ρ_{S4VP} = 1.06 g/ml). Pore formation was achieved by immersing blend films after SVA in pure ethanol at room temperature (T ≅ 21°C) for 1 hour.

1.4. Solvent Vapor Annealing (SVA)

The annealing step was carried out in an automated SVA instrument designed in-house, which was inspired by previous research[33–35] and is briefly described below. The SVA instrument consists of a nitrogen gas source that is split into two lines and connected to separate mass flow controllers (MFCs), controlled by a MKS 946 vacuum system controller that is connected to a computer from which it can receive serial commands. One MFC is connected to a bubbler that holds the solvent of choice and the other is connected directly to a dry "purge" gas line. The bubbler line is then rejoined with the purge line, and both gas streams are mixed before being transported to the annealing chamber. The chamber is aluminum with a removable glass lid and can hold sample sizes up to a full 100 mm diameter wafer. The chamber sits on an Instec TC104 Peltier plate connected to an mK2000 controller, which is used to maintain a constant substrate temperature (18 °C). The film thickness was measured continuously during SVA using a Filmetrics film thickness measurement instrument (Filmetrics F20-UV). A Python script was used to automate control over the polymer volume fraction under swelling using a feedback loop which adjusts the

solvent vapor pressure in the chamber to maintain the measured swelling ratio (i.e swollen film thickness/ dry film thickness) as close as possible to a target value by changing the purge flow rate. The typical standard deviation in the swell ratio about the target value after stabilization at the targeted value is ± 0.0008. The annealing time was defined as the time after reaching the targeted swelling ratio value; the time required to reach this target was approximately 5 min. At the end of the annealing time, the system was quenched by simultaneously reducing the bubbler line flow rate to 0 sccm and increasing the purge gas line flow rate to its maximum (> 100 sccm). Dewetting was not observed in block copolymer or blend films after one or more hours of SVA in acetone at a swell ratio of 1.5 on either clean silicon or brush-treated substrates.

Surface energy contribution estimation

The polar and dispersion components of surface tension are necessary to accurately estimate the interfacial energy between the modified substrate and the BCP and can be related as follows:[36]

$$\gamma_{12} = \gamma_1 + \gamma_2 - \frac{4\gamma_1^{\mathrm{d}}\gamma_2^{\mathrm{d}}}{\gamma_1^{\mathrm{d}} + \gamma_2^{\mathrm{d}}} - \frac{4\gamma_1^{\mathrm{p}}\gamma_2^{\mathrm{p}}}{\gamma_1^{\mathrm{p}} + \gamma_2^{\mathrm{p}}} \qquad \textbf{Eq.1}$$

The subscript 1 represents one of the polymer blocks and the subscript 2 represents a polymer brush, while superscripts "*d*" and "*p*" indicate dispersive and polar components, respectively. This relationship was used to estimate $\gamma_{PS-Substrate}$ and $\gamma_{P4VP-Substrate}$.

The components of the surface tensions for each polymer were estimated from static liquid contact angle measurements on substrates modified with homopolymer brushes using the geometric mean method. A P4VP homopolymer (~6 kg/mol) was used in place of a grafted brush for these measurements. Measurements were performed with an Ossila Contact Angle Goniometer

using deionized water (15 μl) and diiodomethane (15 μl) as test liquids to obtain the polar and dispersive contributions[37], respectively. The surface energies of the different substrates were calculated inserting the contact angles obtained experimentally into the following equation[38]:

$$(1+\cos\theta_t)\gamma_t = 2\left\{(\gamma_t^d\gamma_s^d)^{\frac{1}{2}} + (\gamma_t^p\gamma_s^p)^{\frac{1}{2}}\right\} \quad \textbf{Eq.2}$$

where the subscripts t and s stand for test liquid and substrate respectively.

1.5. Morphological Analysis

The arrangement of BCP domains (e.g., orientation with respect to the substrate) was imaged using scanning electron microscopy (SEM, Hitachi S-4800) at a 10 kV accelerating voltage and transmission electron microscopy (TEM) or scanning TEM (STEM, FEI Talos F200X) coupled with four-quadrant energy dispersive spectroscopy (EDS) mapping acquired in STEM mode using a high angle annular dark field (HAADF) detector operated at 200 kV. SEM images were analyzed using ImageJ to determine pore size and pore density. Samples for TEM and STEM imaging were prepared by a standard in situ lift-out procedure using ion milling performed at 2 keV in a focused ion beam system (FEI Helios G5 UX DualBeam FIB/SEM). Platinum deposited in the FIB system was used as a protective capping layer. In another sample, approximately 4-6 nm of titanium dioxide was deposited by atomic layer deposition at 85 °C using titanium isopropoxide and water as precursors prior to FIB sample preparation, a portion of which deposited on the pore walls down to the substrate interface.

Grazing-incident small-angle X-ray scattering (GISAXS) was performed at the 11-BM Complex Materials Scattering (CMS) beamline at the National Synchrotron Light Source II (NSLS-II). Two-dimensional scattering images were collected using a photon-counting area detector (Dectris Pilatus 2 M), positioned 5.05 m from the sample. The measurements were

conducted with an X-ray beam of 13.5 keV (λ = 0.09184 nm), employing a 10 s integration time at incidence angles of 0.05°, 0.08°, 0.10°, 0.12°, and 0.15°. Data are primarily reported at an incident angle of 0.10°; raw GISAXS patterns at the other angles have been included with the Supporting Information. To convert the data into q-space, silver behenate (AgBH) powder served as a standard. The SciAnalysis toolbox[39] was employed for data analysis.

The porosity of the polymeric films was estimated by spectroscopic ellipsometry as described in the text. The polarization change with the reflected light expressed in terms of amplitude ratio (ψ) and phase difference (Δ) was measured at different incident angles (50°, 60°, 70°, 80°) and fitted using a Cauchy dispersion model to estimate the refractive index (n) and extinction coefficient (k) of the films.

2.7 Metal Oxide Infiltration Synthesis

P4VP domains were selectively infiltrated with alumina and zinc oxide (AZO) using an Atomic Layer Deposition (ALD) system (Cambridge Nanotech, Savannah S100) to provide contrast for SEM imaging in samples without pores. This process was carried out at 85°C using diethyl zinc (DEZ) and trimethylaluminum (TMA) as metal-organic precursors and water as the oxidizing species. The protocol was adapted from the one described previously by Russell et al., in which the precursor exposure time was 5 minutes, during which time the dosage pulse (both TMA and water) was repeated every 30 seconds (total of 10 repeated microdosing pulses).[40,41] The same recipe was used for DEZ and water and repeated for 3 cycles, to ensure that the BCP film is fully infiltrated. Prior to imaging, the samples were partially etched for 40 s at room temperature using an oxygen plasma (21 W; 100 mTorr).

2.8. Solvent Absorption experiments

Solvent absorption experiment similar to the one used by Kim et al.[42] were performed to understand the selectivity of annealing solvents towards the polymers used in this study. Homopolymers with high molar masses were used in order to prevent dewetting during the swelling experiments. Solution of 3 % (w/w) P2VP (855 kg/mol) in 2-methoxyethanol, 3 % (w/w) P4VP (78 kg/mol) in 2-methoxyethanol, 1 % (w/w) PMMA (769 kg/mol) in toluene and 0.5 % (w/w) PS (877 kg/mol) in toluene were spin coated for 30 sec at different angular velocities on cleaned silicon wafers. A spin speed of 5000 rpm was used for P2VP, P4VP and PMMA, while 250 rpm was used for PS, to achieve uniform films with comparable thicknesses (~100 nm). These films were swelled in a completely closed annealing chamber (volume = 423.5 cm^3) with 20 ml of acetone or THF annealing solvent at constant temperature (T = 18°C), and the thickness was recorded as a function of time using an F20-UV. The swelling ratios obtained at 35 min were compared among the different homopolymer to determine the selectivity ratios.

Solvent absorption experiments were also performed on polymer brushes grafted to silicon as described previously. In this case, a deuterium lamp was included in addition to the usual halogen lamp light source, which extends the range of wavelengths for analysis to ~190 nm. This enables more precise film thickness measurements in the range of dry brush thicknesses (down to ~2 nm), but the ultraviolet exposure promotes polymer degradation, particularly in the case of PMMA, which complicates interpretation.

3. Results and Discussion

Nanoporous film fabrication protocol

Our methodology, depicted schematically in **Figure 1a**, consists of a series of steps of substrate functionalization with a polymer "brush" layer (i-iii), polymer blend film blade casting

(iv), automated solvent vapor annealing (v-vi), and P4VP extraction in a selective solvent (vii-viii).

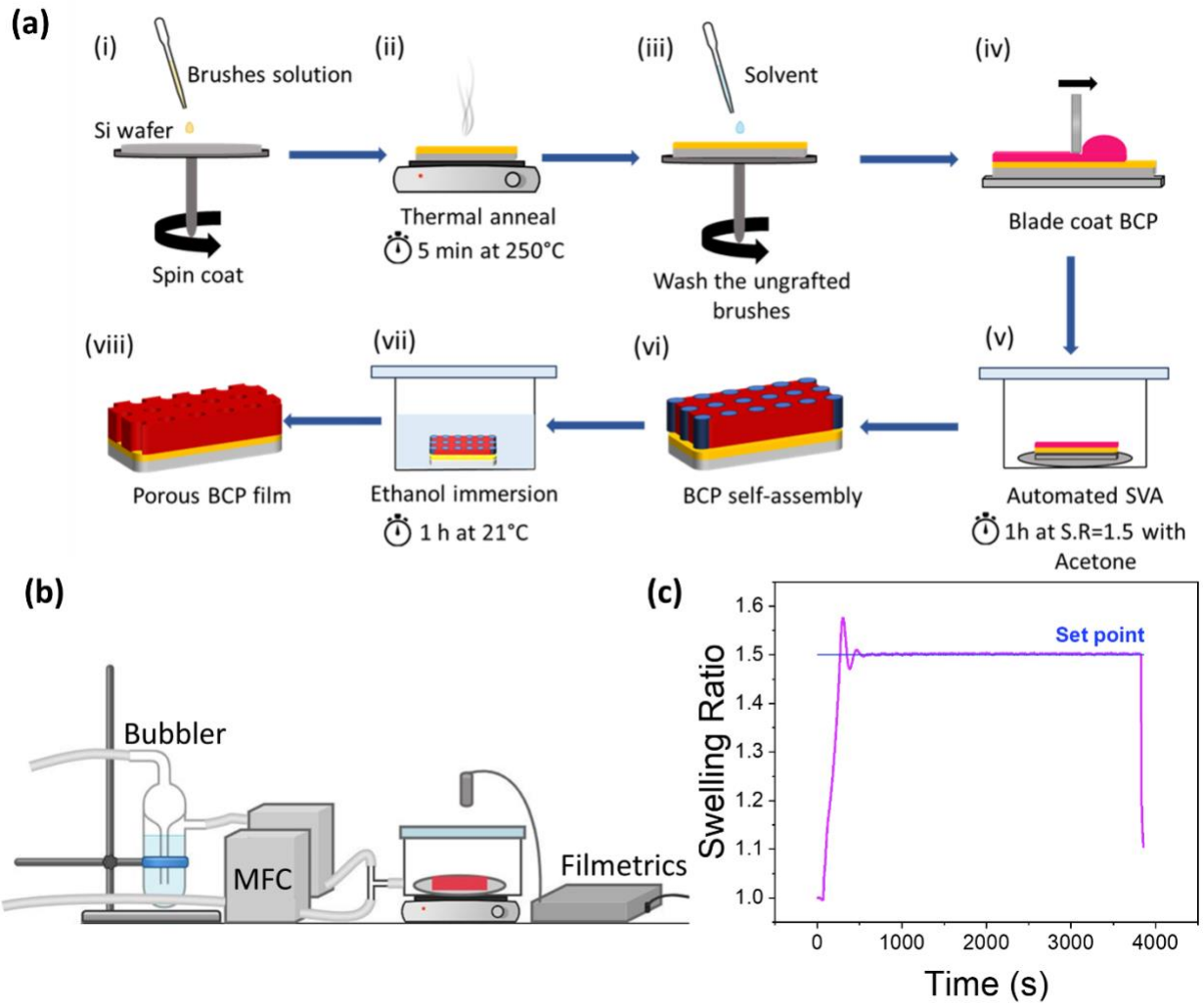

Figure 1. Protocol for nanoporous film fabrication used in this study. **(a)** Schematic illustration of the fabrication process flow. HP brushes are grafted to cleaned substrates by (i) spin-coating films of hydroxy-terminated HPs, (ii) thermal annealing, and (iii) rinsing away excess hydroxy-terminated HP in casting solvent. Thin films of PS-*b*-P4VP BCP blended with P4VP HP are then (iv) cast by blade coating, and (v) induced to assemble vertically-oriented P4VP cylinders by automated SVA. (vi) Immersion in ethanol extracts P4VP HP, yielding (vii) vertically oriented

nanopores. **(b)** Schematic of the automated SVA set up used in this study which consists of a solvent bubbler, mass flow controllers (MFCs), an annealing chamber with temperature controlled by an underlying Peltier plate, and a reflectance-based thickness measurement instrument (Filmetrics F20-UV) to measure swelling during SVA. **(c)** Exemplary automated SVA plot showing the film swelling ratio during a prescribed annealing time (i.e, 1 hour) for the PS-*b*-P4VP systems with acetone, where the pink line represents the measured data and the blue line represents the targeted set point.

To functionalize the substrates, homopolymer brushes (i.e, PS-OH, PMMA-OH, and P2VP-OH) were spin-coated onto cleaned silicon wafer substrates and then baked at 250 °C for 5 minutes under continuous nitrogen purging to graft a monolayer of the homopolymer to the substrates via a dehydration reaction.[43,44] Samples were then rinsed with the neat casting solvent to remove the ungrafted brush polymer and dried by spinning-drying. PS-*b*-P4VP with or without P4VP homopolymer was then cast onto the functionalized substrates by blade coating.[32] This step was performed at various velocities to investigate a range of polymer film thicknesses (~30 nm to ~200 nm).

SVA was then used to facilitate self-assembly of the polymer films into the vertical cylinder morphology with long-range order. The polymer films are swollen with solvent by absorption from an equilibrated solvent vapor. This solvent acts as plasticizer within the film, reducing the glass transition temperature below room temperature and (partially) screening interactions between the two blocks and between the blocks and the substrates.[45] We used an automated flow SVA system, depicted schematically in **Figure 1b**, to ensure precise control over the swelling ratio (SR = swollen film thickness/dry film thickness). In this set-up, flow of a nitrogen carrier gas is used to continually feed solvent vapor into the chamber via a bubbler, while

in situ measurements of the film thickness provide the necessary feedback to automatically control chamber solvent vapor pressure by adjusting dry nitrogen "purge" gas flow. Excellent control of the film swelling ratio is achieved as shown by an example provided in **Figure 1c**, in which SVA was conducted for 1 hour at SR = 1.5 using acetone. Lastly, nanopores were formed in blend films by extracting P4VP homopolymer from the cylinders by immersion in ethanol, a P4VP-selective solvent,[29,46] for 1 hour at ambient temperature.

Assembly of vertical cylinders from a neat PS-*b*-P4VP block copolymer

In the annealing step, the choice of the solvent plays a crucial role in determining cylinder domain ordering and orientation, as the annealing solvent lowers the effective interaction parameter between the polymer blocks and induces preferential block wetting at the free surface of the swollen film, depending on the relative selectivity of the solvent for each polymer block.[45,47] THF (Hansen solubility parameter, δ = 19.4 $MPa^{0.5}$)[48] has been used in the past by Russell et al.[49] for the assembly of vertical cylinders in PS-*b*-P4VP in films with thicknesses on the order of the domain spacing or less. Meanwhile, acetone (Hansen solubility parameter δ = 19.9 $MPa^{0.5}$)[48] has been demonstrated to promote self-assembly of perpendicular lamellae in PS-*b*-P2VP diblock and PS-*b*-P2VP-*b*-PS triblock thin films.[14,50] Based on reported PS and P4VP Hansen solubility parameters[49,51] (δ = 18.6 $MPa^{0.5}$ and δ = 22.2 $MPa^{0.5}$, respectively), we considered acetone to be a potentially viable annealing solvent for PS-*b*-P4VP as well. Solvent vapor sorption experiments were performed using PS and P4VP homopolymers to determine the selectivity ratio of both solvents (**Figure 2**); from these we find the PS/P4VP selectivity ratio is 2.9 for THF and 1.4 for acetone, indicating that the THF is strongly PS-selective while the acetone is only weakly so.

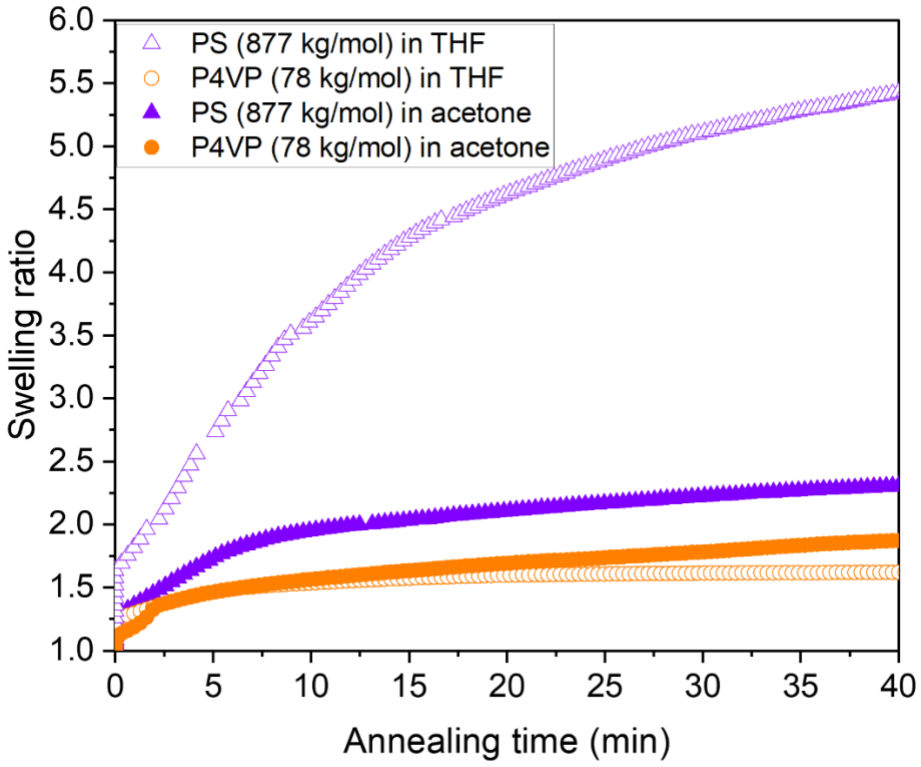

Figure 2. Solvent vapor sorption in a closed chamber (i.e., saturation conditions) as a function of time for PS (877 kg/mol) and P4VP (78 kg/mol) by acetone (filled symbols) or tetrahydrofuran (THF; empty symbols). The swelling ratio is the swollen film thickness divided by the initial dry film thickness.

To assess the effect of SVA using these solvents on cylinder domain orientation, we cast 100-200 nm thick BCP films onto clean bare silicon substrates and conducted SVA for 1 hour at swelling ratios equal to 1.4, 1.5, and 1.6. Films annealed using THF exhibited assembly of predominantly horizontal cylinders across this range, as shown by GISAXS patterns and SEM images (see **Supplementary Information Figures S1**). This is somewhat expected based on the strong PS-selectivity of THF. In contrast, GISAXS characterization of films annealed using acetone revealed similar sized populations of both horizontal and vertical cylinders for SR from

1.4 to 1.5, and an order-disorder transition as the SR is increased from 1.5 to 1.6 (see **Supplementary Information Figures S2**). PS-*b*-P4VP films annealed at SR values less than 1.4 lacked sufficient mobility to assemble a well-ordered cylinder morphology. An SEM of a BCP film annealed at SR = 1.5 for an hour with acetone (after metal oxide infiltration) confirms the presence of both vertical and horizontal cylinders (**Figure 3a and 3b**). Notably, vertical cylinders are most prevalent at the free surface but are absent at the substrate interface. From this we infer that acetone is suitably nonselective to enable assembly of vertical P4VP cylinders in PS-*b*-P4VP films. However, the higher affinity of P4VP for the native silicon oxide interface drives the competing self-assembly of horizontally oriented cylinder domains.

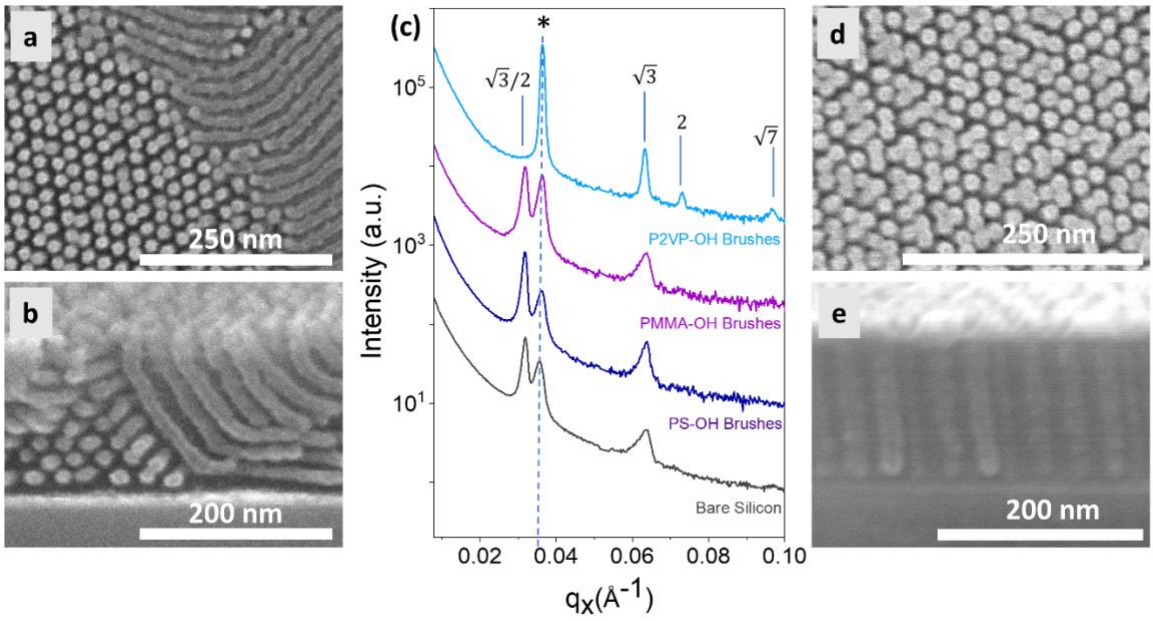

Figure 3. Orientation of P4VP cylinder domains for the neat PS-*b*-P4VP after acetone SVA on substrates functionalized with different brushes. **(a)** Top view and **(b)** cross-section SEM images on bare Si substrates. **(c)** 1D GISAXS pattern linecuts acquired from samples on substrates (bottom to top) with bare silicon and functionalized using PS-OH, PMMA-OH, and P2VP-OH

homopolymer brushes. The dashed line is a guide to the eye to highlight the primary peak associated with vertically-oriented cylinders. The numbers indicate the approximate position of other peaks relative to the primary peak (*). **(d)** Top view and **(e)** cross-section SEM images on substrates functionalized using a P2VP-OH brush. All SEM images were acquired after P4VP-selective metal-oxide infiltration and brief oxygen plasma etching to create domain contrast for imaging.

Based on their straightforward synthesis and wide availability, we used homopolymer brush grafting for surface modification to achieve the appropriately balanced interfacial interactions. General principles for their selection are lacking, however. As a heuristic, we tested a hydroxy-terminated PMMA brush (PMMA-OH) based on the previously demonstrated neutral affinity of PMMA for PS and P2VP,[52] with the assumption that it may be applicable to PS-*b*-P4VP as well. We also investigated a P2VP-OH brush considering its chemical similarities to the P4VP block. The ideal "neutral" condition that enables vertical BCP domain orientation is generally attained when the difference in interfacial energy (γ) between the two blocks and the functionalized substrate is minimized.[23,37] In our case, this corresponds to the condition in which $|\gamma_{P4VP-Brush} - \gamma_{PS-Brush}| \approx 0$. Based on measured water and diiodomethane contact angles reported in **Table 1**, we calculated the magnitude of this difference in interfacial energies using the method of Wu[36] to obtain 5.38 mN/m and 8.47 mN/m for PMMA-OH and P2VP-OH, respectively (details of the calculation, are described in the **Methods**). As expected, these magnitudes are less than the interfacial energy between PS and P4VP ($\gamma_{PS-P4VP}$ = 13.1 mN/m). However, polymer-brush interactions are less balanced on P2VP-OH than on PMMA-OH, suggesting that vertical domain orientation should be less likely in the former case.

Table 1. Water and diiodomethane contact angles, dispersive and polar contributions of the surface energy and surface energies for the different homopolymer substrates.

Substrate	θ_{water} (degrees)[a]	$\theta_{Diiodomethane}$ (degrees)[b]	$\gamma_s^d \left(\frac{mN}{m}\right)$[c]	$\gamma_s^p \left(\frac{mN}{m}\right)$[d]	$\gamma \left(\frac{mN}{m}\right)$[e]
PS-OH	89.03	34.76	41.53	0.84	42.37
PMMA-OH	69.06	37.34	34.69	9.10	43.79
P2VP-OH	61.28	21.56	39.76	11.35	51.11
P4VP	53.22	10.89	40.62	15.42	56.04

[a] Water contact angle measurements perform on the functionalized silicon substrates
[b] Diiodomethane contact angle measurements perform on the functionalized silicon substrates
[c] Dispersive contribution of the interfacial energies of the functionalized silicon substrates calculated using equation 2 where γ_t^d and γ_t^p for water and diiodomethane taken from elsewhere[53]
[d] Polar contribution of the interfacial energies of the functionalized silicon substrates calculated using equation 2 where γ_t^d and γ_t^p for water and diiodomethane taken from elsewhere[53]
[e] Interfacial energies of the functionalized silicon substrates.

GISAXS patterns acquired from neat PS-*b*-P4VP films after SVA at SR = 1.5 for 60 minutes were used to characterize the orientation of cylinder domains on substrates with different brushes. Samples functionalized using PMMA-OH and P2VP-OH were evaluated based on the above discussion. As comparative controls, we also characterized samples functionalized using PS-OH along with bare silicon samples. Horizontal linecuts along the scattering vector perpendicular to the plane of incidence, q_x, from GISAXS patterns acquired from these samples are shown in **Figure 3c**. A primary scattering peak within the Yoneda band is associated with

vertically oriented cylinders (q_x*). Meanwhile, the presence of horizontal cylinders is associated with a peak at $q_x \approx q_x^* \sqrt{3}/2$.[54,55] The relative amount of vertical and horizontal cylinders can then be assessed by analyzing linecuts along q_x that encompass both peaks (centered at q_z = 0.03 Å^{-1}, integrated over a width $d_{q_z} = 0.04$). We note that the GISAXS patterns were acquired at α = 0.1°, above the critical angle of the PS-*b*-P4VP system ($\alpha_c \approx 0.089°$), and thus contain information about the entire thickness of the films rather than just the surface.

As expected by the selectivity of the oxidized Si substrate for P4VP, the linecut for bare silicon exhibits prominent peaks associated with both vertical and horizontal cylinders. We note that a higher-order peak at $q_x \approx q_x^* \sqrt{3}$ is typical for samples with either horizontal or vertical cylinders. The PS-functionalized substrate similarly exhibits two peaks, indicating a substantial fraction of horizontal cylinders as well, which is expected based on the selectivity of the PS brush for the PS matrix phase. Interestingly, peaks associated with both vertical and horizontal cylinders having near-equal amplitude are also present for the GISAXS linecut corresponding to the PMMA-functionalized substrate, indicating large populations of both vertical and horizontal cylinders despite the expected minimal interfacial energy difference with the two blocks. Most surprisingly, the film cast onto a P2VP-functionalized substrate assembled into well-ordered vertical cylinders, as evidenced by a complete absence of a horizontal cylinder peak at $q_x \approx q_x^* \sqrt{3}/2$ and the presence of higher order peaks at $q_x \approx q_x^* \sqrt{3}, 2q_x^*$ and $q_x^* \sqrt{7}$ that are consistent with a hexagonal symmetry. The vertical cylinder orientation after acetone SVA on P2VP-functionalized substrates is corroborated by SEM images (**Figure 3d and 3e**) from a film processed in the same way, taken after metal oxide infiltration and etching. We note that the existence of horizontally ordered cylinders on substrates not functionalized with P2VP is also clear in the two-dimensional GISAXS patterns corresponding to the curves shown in **Figure 3c**, which reveal peaks at larger q_z that

correspond to a scattering pattern for cylinders oriented with the (10) planes parallel to the substrate (**Supporting Information, Figure S3b**). Though the vertical cylinder orientation observed here on P2VP functionalized substrates is for films obtained by blade casting, we find that it is also achieved for PS-*b*-P4VP films deposited by spin casting on P2VP functionalized substrates that are annealed the same way (Supporting Information, **Figure S4a**).

To better understand the origins of the different cylinder orientations on PMMA- and P2VP-functionalized substrates, we used GISAXS to characterize PS-*b*-P4VP films on both substrates with SVA quenched 0 (~1 s), 5, 10, 20, and 30 minutes after reaching the target SR of 1.5. The time required for the film to reach the target SR is approximately 5 minutes. Linecuts from corresponding GISAXS patterns (following the same protocol as described above) for films on PMMA-functionalized and P2VP-functionalized substrates are shown in **Figure 4a and 4b**, respectively. In **Figure 4a**, it is apparent from the absence of a horizontal cylinder peak at $q_x^*\sqrt{3}/2$ and the presence of higher order peaks at $q_x^*\sqrt{3}$, $2q_x^*$ and $q_x^*\sqrt{7}$ that nearly all the cylinders are vertical immediately upon reaching SR = 1.5 on the PMMA-functionalized substrate. However, as SVA continues, the horizontal cylinder peak progressively increases in magnitude at the expense of the vertical cylinder peak, indicating a gradual reorientation of cylinders. In contrast, the GISAXS patterns associated with well-ordered vertically oriented cylinders remains essentially unchanged as annealing proceeds on P2VP-functionalized substrates (**Figure 4b**). Thus, vertical cylinders initially assemble on substrates functionalized with either brush, but this orientation is an unstable configuration on PMMA-functionalized substrates. Slight shifts in peak position to both higher and lower q_x are visible as annealing time increases. These reflect deviations in repeat spacing of only ~0.2 nm (~1%) or less and can be attributed to small oscillations in swollen film thickness about the setpoint, especially at short times (< 10 min) before full stabilization.

Importantly, we note that analysis of GISAXS patterns acquired from films on PS-functionalized substrates with SVA quenched at the same times show that vertical cylinder orientation is never dominant in that case (**Supporting Information Figure S5**).

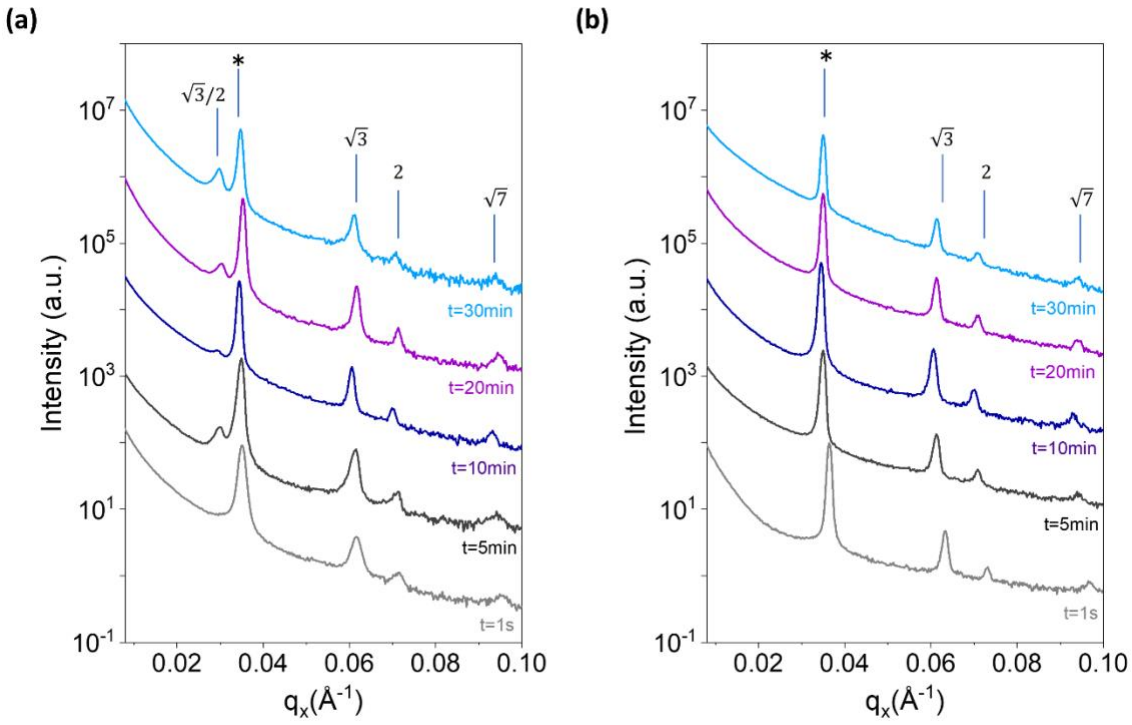

Figure 4. GISAXS characterization of the domain orientation in PS-*b*-P4VP films cast on PMMA- and P2VP-functionalized substrates after SVA with acetone for several durations (1 s, 5 min, 10 min, 20 min, 30 min). One-dimensional GISAXS linecuts were acquired from samples cast on **(a)** PMMA-functionalized and **(b)** P2VP-functionalized substrates.

We speculate that the instability of vertically oriented cylinders on PMMA-functionalized surfaces may be attributed to the preferential swelling of PMMA by acetone compared to all other homopolymers studied in this report (**Figure 5**). Acetone swells P2VP to an extent that is intermediate between PS and P4VP, and may therefore be considered near-neutral for PS, P2VP, and P4VP. Based on the dilution approximation[13] and the Helfand-Tagami relation,[56] acetone

screening of polymer interactions will then reduce the effective magnitudes of $\gamma_{P4VP-P2VP}$ and $\gamma_{PS-P2VP}$ to a similar extent, allowing greater interpenetration of PS and P4VP chains with the P2VP underlayer during SVA relative to dry conditions. In contrast, acetone swells PMMA selectively based on the swelling ratio of more than 3 compared to ~2 or less for the other three polymers in Figure 4. The selective PMMA swelling by acetone will reduce PMMA interpenetration with the two blocks during SVA, rendering a "harder" block-brush interface.[57] Block-brush interpenetration has been theoretically shown to enhance stability of vertical domains by enabling localized chain rearrangement that minimizes less-favorable block-brush contacts.[57,58] The reduced interpenetration of a harder block-brush contact is therefore expected to destabilize vertical domain orientation. The effective neutrality of the polymer-grafted substrate interface may be enhanced with increases solvent swelling (higher SR) if the solvent swells all polymers in the system to a similar extent; in contrast, if any one of the polymers is swollen selectively, the neutrality may be diminished. Importantly, we note that block-brush interpenetration alters the effective boundary condition at the film-substrate interface and does not have to be large with respect to the total film thickness to have a significant effect on the cylinder domain orientation. Thus, the swelling of the underlayer by the SVA solvent must be considered when assessing its efficacy for controlling domain orientation, underscoring the higher complexity of designing SVA versus thermal annealing processes. Acetone vapor swelling experiments performed on P2VP-OH and PMMA-OH monolayers grafted to silicon (Supporting Information **Figure S6**) strongly corroborate the results observed in Figure 5. Poor spectra fitting adds uncertainty for the thickness measurements of swollen PMMA-OH, however. Furthermore, these measurements required additional ultraviolet illumination in spectral reflectance measurements for sufficient precision at brush thicknesses; direct inference from these measurements must therefore be treated with

caution, as the ultraviolet illumination can degrade the polymer (especially for PMMA), even if much of it is attenuated by the chamber cover glass.

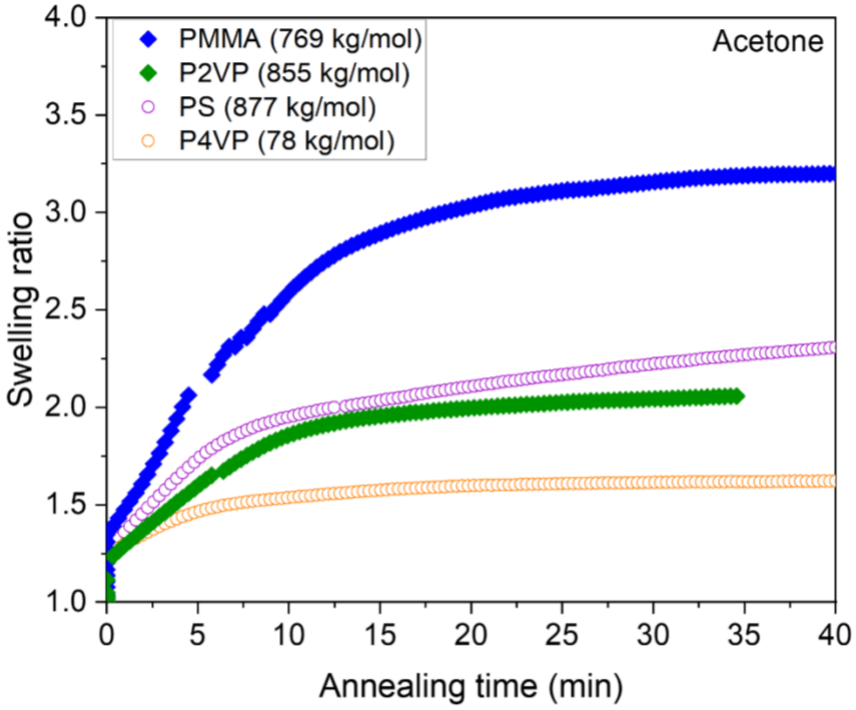

Figure 5. Sorption of acetone solvent vapor in a closed chamber (i.e., saturation conditions) as a function of time for PMMA (769 kg/mol), P2VP (855 kg/mol), PS (877 kg/mol) and P4VP (78 kg/mol). The swelling ratio is the swollen film thickness divided by the initial dry film thickness.

further understand the swelling of the different homopolymer brushes, we determined the graft density (σ) as

$$\sigma = \frac{\rho N_A h_{dry}}{M_n} \qquad \textbf{Eq.3}$$

where ρ is the bulk density of the homopolymer (1.19 g/cm^3, 1.05 g/cm^3 and, 1.15g/cm^3 for PMMA, PS, and P2VP, respectively), N_A is Avogadro's number, h_{dry} is the brush thickness measured with the spectroscopic ellipsometry and M_n is the number average molar mass of the

homopolymer.[59,60] This calculation yields grafting densities of 0.45 nm^{-2}, 0.50 nm^{-2}, and 0.56 nm^{-2} for PMMA-OH, PS-OH, and P2VP-OH brushes, respectively. Based on these σ values, we may presume the brushes are in a high density regime, where the polymer chains exhibit a more stretched and upright conformation compared to the mushroom regime (i.e. low graft density).[59] These brush chains may nevertheless swell by absorbing solvent; indeed, the calculated contour lengths for PS-OH, PMMA-OH, and P2VP-OH are 14.4, 16.3, and 18.3 nm, respectively.[59–61] This implies the maximal possible swelling of the dry brushes significantly exceeds the SR values employed in our experiment. Moreover, acetone at fractions greater 50% (SR $>$ 2) has been incorporated into solvent-immersed, surface-grafted PMMA-OH brushes at similar grafting densities.[59] We note also that the lower grafting density of the PMMA-OH compared to P2VP-OH should enable it to swell more in acetone, since less chain stretching is necessary to incorporate the same volume of solvent at lower grafting densities. Acetone is a good solvent for PMMA but not PS or P4VP, and these solvation differences may drive selective acetone incorporation into the PMMA-OH underlayer at the interface with the overlying PS-*b*-P4VP film. As described above, this selective swelling would in turn reduce interpenetration between the brush and the polymer blocks. On the other hand, acetone is not a good solvent for P2VP, and our absorption experiments reveal comparable swelling among PS, P4VP, and P2VP that allows more chain interpenetration at the brush-block interfaces.

We also evaluated the effect of film thickness on assembled cylinder orientation using acetone SVA on P2VP-functionalized substrates. In very thin films ($h \sim L_0$), entropic penalties arising from incommensurability between film thickness and the spacing between horizontally oriented domains can help maintain vertical domain orientation in spite of weakly-preferential film interfaces.[62,63] This entropic penalty decreases as film thickness is increased, underscoring the need

to properly balance interfacial energies at both substrate and free interfaces to maintain vertical orientation at high aspect ratios ($h/L_0 \gg 1$). To assess the efficacy of vertical orientation of the acetone SVA/P2VP-OH brush combination for vertical cylinder assembly, we blade coated samples with gradient film thicknesses and characterized them by both GISAXS and SEM. The presence of the primary peak and higher-order peaks at $q_x^*\sqrt{3}$, $2q_x^*$ and $q_x^*\sqrt{7}$ in the scattering patterns of the BCP film in a thickness range from ~30 nm to ~200 nm, as shown in **Figure S7**, indicates that a vertical cylinder morphology is preserved throughout the thickness range. This is corroborated by SEM images from assembled films with thicknesses equal to ~60, ~100, and ~170 nm (**Figure S7**).

Tuning pore sizes through homopolymer blending

Blending asymmetric cylinder-forming BCPs with HPs that are chemically identical or enthalpically compatible with the minority block is a powerful approach to modify cylinder domain size and to generate pores by cylinder phase decomposition or HP extraction. While it has been shown that the extent of domain size increase is a function of both HP volume fraction and molar mass,[5,29,64] less attention has been devoted to the effects these HP properties have on domain orientation. The assembly of high aspect ratio cylinder domains demonstrated here presents an opportunity to investigate the relationships between blend composition and film morphology more systematically.

We investigated blends of the same PS-*b*-P4VP BCP with linear P4VP HPs having three different molar masses: 3 kg/mol, 6 kg/mol, and 12 kg/mol, respectively. These HP molar masses, and therefore chain lengths, exemplify three notable regimes in binary BCP/HP blends, which are defined by the relative degrees of polymerization between the HP and the minority block ($\alpha = N_{P4VP,homopolymer}/N_{P4VP,block}$).[65] Blends in which $\alpha < 1$ (3 kg/mol HP) are considered to be in the "wet

brush" regime since the HP is solubilized by the minority domain and can distribute more uniformly within the domain to maximize translational entropy. Blends in which $\alpha \sim 1$ (6 kg/mol) are considered "dry brush". Here, the HP is solubilized within the minority domain but almost entirely segregates to the domain center to maximize conformational entropy. Finally, blends in which $\alpha >> 1$ (12 kg/mol) tend to macrophase separate from the microphase separated morphology entirely.

The top view and cross-section (insets) SEM images from blends with the three molar masses at two distinct HP volume fractions (ϕ_{P4VP}) are presented in **Figure 6**. When ϕ_{P4VP} is 0.09 (**Figure 6a-c**), vertically-oriented cylinders form for all molar mass homopolymers. However, blends with HP of each molar mass exhibit very different self-assembled morphologies as ϕ_{P4VP} is increased to 0.19 (**Figure 6d-f**). Large spherical objects are observed for 12 kg/mol P4VP HP (**Figure 6f**). We interpret this as evidence of incipient macrophase separation, an expected result given the large α for this blend. In contrast, the 3 kg/mol P4VP HP induces a vertical-to-horizontal cylinder reorientation as ϕ_{P4VP} is increased to 0.19 (**Figure 6d**). This surprising result can be explained by the tendency for wet brush HPs to enrich film surfaces and interfaces. It is well recognized that shorter polymers in a polymer blend will preferentially segregate to film surfaces as the comparative entropy loss is smaller,[66] and Toth et al. have shown that wet brush HP enrichment at film surfaces in BCP/HP blends can generate wetting layers that drive a vertical-to-horizontal change in domain orientation.[67] Blends with the 6 kg/mol P4VP HP, on the other hand, continue to assemble into well-ordered vertical cylinders when ϕ_{P4VP} is increased to 0.19 (**Figure 6e**). Jeong et al. have shown that strong confinement of dry brush homopolymers to the center of cylinder domains reinforces vertical domain orientation in thin films,[68] which is consistent with the assembly for the 6 kg/mol P4VP HP blend observed here. A schematic representation of the

distribution of P4VP HP at ϕ_{P4VP} = 0.09 (i.e., at a volume fraction lower than the onset of domain reorientation) within and in the vicinity of a cylindrical domain is provided in **Figure S8.**

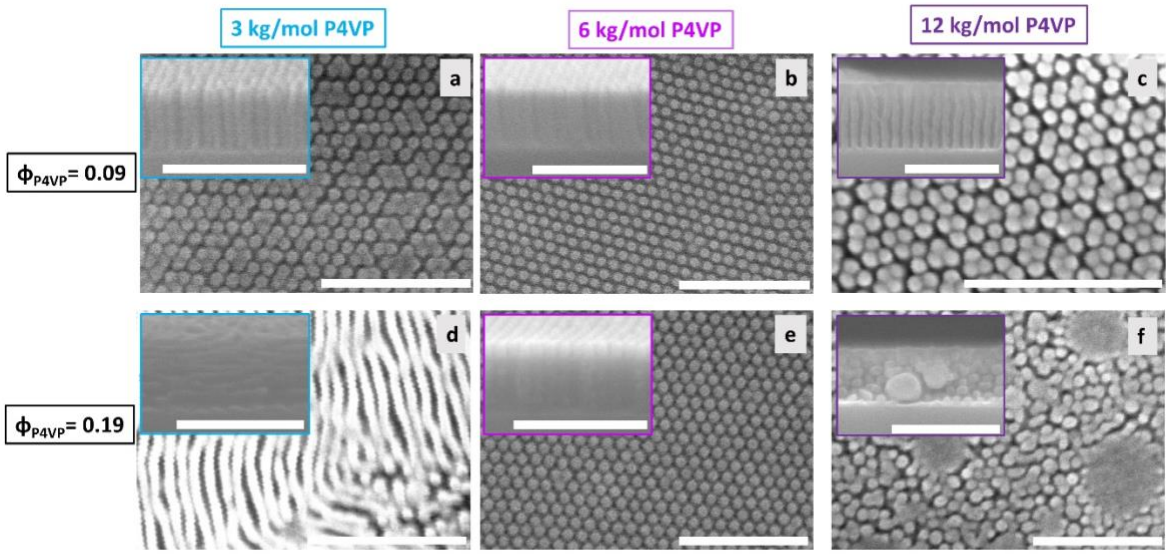

Figure 6: Top and cross- sectional view SEM images demonstrating the effect of P4VP HP molar masses and volume fraction (ϕ_{P4VP}) on domain morphology in PS-*b*-P4VP/P4VP binary blends after acetone SVA on P2VP-functionalized substrates. Top row: SEMs of blends with ϕ_{P4VP} = 0.09 for HP molar masses equal to **(a)** 3 kg/mol, (b) 6 kg/mol, and **(c)** 12 kg/mol. Bottom row: SEMs of blends with ϕ_{P4VP} = 0.19 for HP molar masses equal to **(d)** 3 kg/mol, **(e)** 6 kg/mol, and **(f)** 12 kg/mol. Inset SEM images show film cross-sections. All SEM images were acquired after P4VP-selective metal-oxide infiltration and brief oxygen plasma etching to create domain contrast for imaging. All scale bars denote 250 nm.

These trends are supported by GISAXS characterization, where the presence of the primary peak and higher order peaks at $q_x^*\sqrt{3}$, $2q_x^*$ and $q_x^*\sqrt{7}$ in the GISAXS scattering patterns confirms

the vertical orientation of the cylinder in a hexagonal lattice for blends with ϕ_{P4VP}=0.09 at all three HP molar masses (see **Supplementary information Figure S9)**. The same plot indicates that vertical cylinders are preserved for blends up to at least ϕ_{P4VP} = 0.19 only if using the 6 kg/mol P4VP HP. In addition, blends with the 6 kg/mol P4VP HP exhibit a vertical cylinder morphology in films with thicknesses ranging from ~40nm to ~170 nm (characterized at ϕ_{P4VP} = 0.09, see **Supplementary Information Figure S10)**. Our results show that blended HP molar mass plays a decisive role in determining cylinder orientation when the films are annealed under conditions in which block-surface interfacial energies are nearly balanced, as described here. Careful HP selection is thus necessary to achieve the broadest range of tunabilities for pore diameters and aspect ratios.

We have also characterized the scaling of pore size with ϕ_{P4VP}. We focus on the 6 kg/mol P4VP HP given the superior stability of vertically-oriented cylinders in this case. Histograms of pore diameters generated by P4VP HP extraction using ethanol, as described previously, with blends with ϕ_{P4VP} = 0.05, 0.09, 0.19, and 0.28 are shown in **Figure 7a**. The corresponding mean pore diameters, domain spacing (cylinder-to-cylinder) and measured pore density for these blends are provided in **Table 2**. Of note, a ϕ_{P4VP} of at least ~0.05 was necessary to obtain consistently open pores, but the pore diameter is nearly 10 nm at this volume fraction, almost equal to the pore diameter for ϕ_{P4VP} = 0.09. At the other extreme (ϕ_{P4VP}= 0.28), a broad pore diameter distribution is observed at the onset of HP macrophase separation from the PS-*b*-P4VP. We note that the vertical pores span the entire film thickness, as confirmed by TEM cross-section images of a ~170 nm thick porous film formed from a blend with ϕ_{P4VP} = 0.05 (**Figure 7b** and **7c**). Here, platinum (Pt) deposited as a protective encapsulant for cross-sectioning coats the pore walls down to the substrate interface. **Figure S11** in the Supporting Information provides further evidence for

vertical pores spanning the entire film thickness in a cross-sectional high angle annular dark field (HAADF) STEM image and accompanying STEM EDS maps in which a thin titanium dioxide layer was deposited onto pore walls by ALD prior to STEM sample preparation. Titanium dioxide extends the whole length of the pores to the native silicon dioxide layer on the silicon substrate. Additional cross-section SEM images illustrating the presence of vertical pores spanning the entire film thickness for blends with varied HP volume percentages are provided in **Figure S12**. This was also verified for spin coated PS-b-P4VP blend films with 0.09 volume fraction of 6kg/mol P4VP, as shown in **Figure S4b,c**.

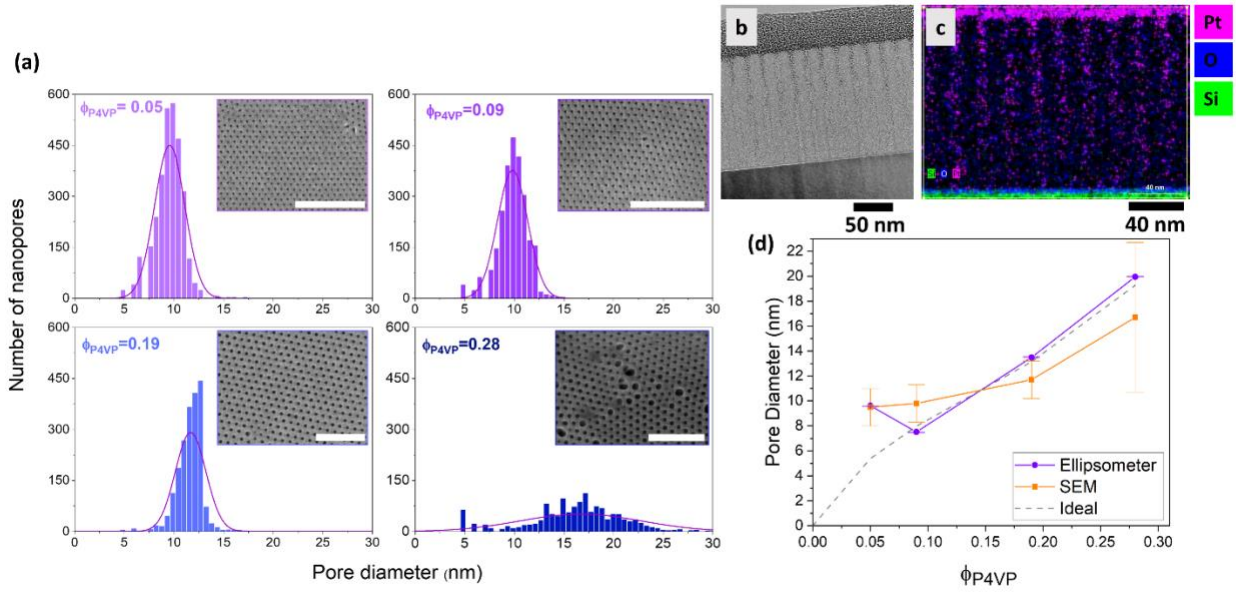

Figure 7. Characterization of mean vertical pore diameter after HP extraction with ethanol for PS-*b*-P4VP blends with 6 kg/mol P4VP homopolymer at different volume fractions. **(a)** Histograms of the pore diameter distribution as a function of homopolymer volume fraction. Insets: Corresponding top view SEM images (scale bars denote 250 nm). **(b)** TEM image and **(c)** corresponding overlaid Pt (magenta), oxygen (O, blue) and silicon (Si, green) STEM EDS maps

of a PS-*b*-P4VP /P4VP blend films (ϕ_{P4VP} = 0.05) after ethanol immersion. The Pt is deposited as a protective top layer for TEM sample preparation and its presence on the pore walls down to the substrate interface indicates that the pores are vertically oriented and open. **(d)** Mean pore diameters as a function of the homopolymer volume fraction calculated by direct analysis of SEM images (orange squares) and from ellipsometer measurements (purple circles) of the film porosity using equation 4. An "ideal" curve (gray dashed line), which estimates the mean diameter from equation 4 assuming the total porosity $\phi = \phi_{P4VP}$, is included for comparison.

Table 2. Variation of the average pore diameter, center-to-center domain spacing (L_0) and pore density in the PS-*b*-P4VP films as a function of homopolymer volume fractions added in the blends.

ϕ_{P4VP}	Average Pore diameter (nm)[a]	L_0 (nm)[b]	L_0 (nm)[c]	Pore Density (cm^{-2})[d]
0.05	9.5 ± 1.5	23.0	22.4	$2.2 \cdot 10^{11}$
0.09	9.8 ± 1.5	26.0	24.5	$1.8 \cdot 10^{11}$
0.19	11.7 ± 1.5	28.9	27.3	$1.4 \cdot 10^{11}$
0.28	16.7 ± 6	37.0	33.3	$9.6 \cdot 10^{10}$

[a] Average pore diameters estimated through SEM images using ImageJ and the uncertainty represented by standard deviation
[b] Cylinder-to-cylinder domain spacing estimated through SEM images using ImageJ
[c] Cylinder-to-cylinder domain spacing calculated by fitting the GISAXS scattering patterns to obtain the position of q_x^*, where $L_0 = 4\pi/q_x^*\sqrt{3}$
[d] Pore density estimated using ImageJ as pore counts divided by area in SEM images

The pore diameters calculated by analysis of SEM images only represent pores at the film surface and may be affected by imaging conditions. To provide a more robust estimate of porosity

across the entire film volume, we applied the ellipsometric measurement method described by Galy et al.,[69] which estimates film porosity from measured refractive indices by the equation

$$\phi = \frac{n_{eff}^2 - n_c^2}{n_d^2 - n_c^2} \qquad \textbf{Eq.3}$$

where n_{eff} is effective refractive index of the two-phase composite, n_d is the refractive index of the dispersed phase (i.e, $n \approx 1$ for air in this case), n_c is the refractive index of the continuous phase (i.e, a BCP film without pores) and ϕ is the total porosity of the BCP film. This estimated porosity can be converted to an effective mean pore diameter (d_{eff}) using the pore density measured by SEM (P_d) by the following equation:

$$d_{eff} = \sqrt{\frac{4\phi}{\pi P_d}} \qquad \textbf{Eq.4}$$

The diameters obtained from SEM and ellipsometry are plotted together as a function of ϕ_{P4VP} in **Figure 7d**. For comparison, we also plot an "ideal" pore diameter (gray dashed line), which assumes that the volume of P4VP HP is entirely responsible for the pore size, calculated here using equation 4 by replacing the porosity measured by ellipsometry with ϕ_{P4VP} (i.e., $\phi = \phi_{P4VP}$). In comparison, the mean pore diameters measured by ellipsometry nearly match the ideal expectations from ϕ_{P4VP}= 0.09 to 0.28, while SEM image analysis indicates a less significant change in pore diameter at the film surface. However, both SEM and ellipsometry confirm a higher-than-expected pore diameter at ϕ_{P4VP}= 0.05. This is likely a consequence of "domain reconstruction" induced by selective swelling of the P4VP block chains by ethanol,[27,70] which generates an osmotic pressure causing a modest increase in the film thickness and concomitant volume expansion.[28] Rapid drying upon removal from ethanol then leads to collapse of the P4VP chains on the film and pore surfaces, leaving a through-film pore in the unoccupied volume. Wei

et al. found that pores generated from vertical cylinders in PS-*b*-P2VP/P2VP blends by immersion in ethanol (also selective for P2VP) arise due to both domain reconstruction (polymer "swelling") and HP extraction ("dissolution").[30] HP extraction is the main determinant of the pore diameter at high HP fractions, while the reconstruction mechanism contributes significantly to determining the pore diameter at low HP fractions, leading to larger pores than would be expected based on HP extraction alone. Based on this, we infer that the relatively large pore diameters for our PS-*b*-P4VP/P4VP blends with ϕ_{P4VP} = 0.05 are a product of domain reconstruction.

4. Conclusion

This study demonstrates the robust fabrication of well-ordered, self-assembled arrays of vertical nanopores in thin films of asymmetric PS-*b*-P4VP blended with P4VP homopolymers, with diameters tunable to less than 10 nm and aspect ratios reaching ~10. The vertical orientation of the morphology in these thin films is achieved by the combination of SVA using acetone with precisely controlled annealing conditions and substrate functionalization using a P2VP-OH homopolymer. Comparison between assembled cylinder orientations on P2VP- and PMMA-functionalized substrates as SVA progresses shows that solvent-underlayer interactions influence domain orientation considerably. It is therefore not practical to independently select the SVA solvent and the underlayer. We also demonstrate the importance of P4VP HP molar mass selection in PS-*b*-P4VP/P4VP blends for maintaining self-assembled morphologies obtained through optimization of a neat PS-*b*-P4VP while ensuring maximum pore size tunability. Our results provide relevant design rules for the fabrication of thin films with high-aspect ratio nanopores by self-assembly of a canonical high χ BCP system, with a variety of potential applications ranging from biomedicine to energy storage devices and the semiconductor nanopatterning.

Supporting Information.

The following files are available free of charge.

GISAXS pattern linecuts and SEM images Figure S1-S2, GISAXS 2D patterns Figure S3, SEM images Figure S4, GISAXS pattern linecuts Figure S5, acetone absorption curves for PMMA-OH and P2VP-OH Figure S6, GISAXS pattern linecuts and SEM images Figure S7, schematic representation of the distribution of P4VP homopolymer Figure S8, GISAXS pattern linecuts Figures S9-S10, HAADF STEM image and STEM EDS maps Figure S11, SEM images Figure S12, folder containing: raw GISAXS patterns at the various angles arranged into subfolders related to the respective figures and calculations, masks used, and an Excel spreadsheet with a description of each sample. This folder is publicly available on the Web at Materials Data Facility (https://doi.org/10.18126/4fsm-dj55)

AUTHOR INFORMATION

Corresponding Authors

*gdoerk@bnl.gov

Author Contributions

B.B., and S.C. performed experiments. B.B. analyzed data. J.W. developed the Python script for SVA automation. E.T. and R.L. assisted with GISAXS measurements. K.K. performed transmission electron microscopy and related sample preparation. S.K. and G.D. supervised the work. The manuscript was written through contributions of all authors. All authors have given approval to the final version of the manuscript.

Acknowledgment

This research used the Materials Synthesis and Characterization facility, the Electron Microscopy facility and the X-ray scattering partner user program at the Center for Functional Nanomaterials (CFN) and the 11-BM end station of the National Synchrotron Light Source II (NSLS-II), which are U.S. Department of Energy (DOE) Office of Science User Facilities, at Brookhaven National Laboratory under Contract No. DE-SC0012704. S.C., B.B., and G.S.D. were supported by a DOE Early Career Research Program grant.

References

(1) Ruiz, R.; Kang, H.; Detcheverry, F. A.; Dobisz, E.; Kercher, D. S.; Albrecht, T. R.; De Pablo, J. J.; Nealey, P. F. Density Multiplication and Improved Lithography by Directed Block Copolymer Assembly. *Science* **2008**, *321* (5891), 936–939. https://doi.org/10.1126/science.1157626.

(2) Kuschlan, S.; Chiarcos, R.; Laus, M.; Pérez-Murano, F.; Llobet, J.; Fernandez-Regulez, M.; Bonafos, C.; Perego, M.; Seguini, G.; De Michielis, M.; Tallarida, G. Periodic Arrays of Dopants in Silicon by Ultralow Energy Implantation of Phosphorus Ions through a Block Copolymer Thin Film. *ACS Appl. Mater. Interfaces* **2023**, *15* (50), 57928–57940. https://doi.org/10.1021/acsami.3c03782.

(3) Esmeraldo Paiva, A.; Gerlt, M. S.; Läubli, N. F.; Prochukhan, N.; Baez Vasquez, J. F.; Kaminski Schierle, G. S.; Morris, M. A. High Aspect Ratio Nanoscale Pores through BCP-Based Metal Oxide Masks and Advanced Dry Etching. *ACS Appl. Mater. Interfaces* **2023**, *15* (50), 57960–57969. https://doi.org/10.1021/acsami.3c09863.

(4) Greil, S.; Rahman, A.; Liu, M.; Black, C. T. Gas Transport Selectivity of Ultrathin, Nanoporous, Inorganic Membranes Made from Block Copolymer Templates. *Chem. Mater.* **2017**, *29* (21), 9572–9578. https://doi.org/10.1021/acs.chemmater.7b04174.

(5) Yang, S. Y.; Ryu, I.; Kim, H. Y.; Kim, J. K.; Jang, S. K.; Russell, T. P. Nanoporous Membranes with Ultrahigh Selectivity and Flux for the Filtration of Viruses. *Advanced Materials* **2006**, *18* (6), 709–712. https://doi.org/10.1002/adma.200501500.

(6) Zhou, C.; Segal-Peretz, T.; Oruc, M. E.; Suh, H. S.; Wu, G.; Nealey, P. F. Fabrication of Nanoporous Alumina Ultrafiltration Membrane with Tunable Pore Size Using Block Copolymer Templates. *Adv Funct Materials* **2017**, *27* (34), 1701756. https://doi.org/10.1002/adfm.201701756.

(7) Han, K. H.; Seok, J. Y.; Kim, I. H.; Woo, K.; Kim, J. H.; Yang, G. G.; Choi, H. J.; Kwon, S.; Jung, E. I.; Kim, S. O. A 2D Ultrathin Nanopatterned Interlayer to Suppress Lithium Dendrite Growth in High-Energy Lithium-Metal Anodes. *Advanced Materials* **2022**, *34* (34), 2203992. https://doi.org/10.1002/adma.202203992.

(8) Lee, J. I.; Cho, S. H.; Park, S.-M.; Kim, J. K.; Kim, J. K.; Yu, J.-W.; Kim, Y. C.; Russell, T. P. Highly Aligned Ultrahigh Density Arrays of Conducting Polymer Nanorods Using Block Copolymer Templates. *Nano Lett.* **2008**, *8* (8), 2315–2320. https://doi.org/10.1021/nl801105s.

(9) Han, E.; Stuen, K. O.; La, Y.-H.; Nealey, P. F.; Gopalan, P. Effect of Composition of Substrate-Modifying Random Copolymers on the Orientation of Symmetric and Asymmetric Diblock Copolymer Domains. *Macromolecules* **2008**, *41* (23), 9090–9097. https://doi.org/10.1021/ma8018393.

(10) Han, E.; Stuen, K. O.; Leolukman, M.; Liu, C.-C.; Nealey, P. F.; Gopalan, P. Perpendicular Orientation of Domains in Cylinder-Forming Block Copolymer Thick Films by Controlled Interfacial Interactions. *Macromolecules* **2009**, *42* (13), 4896–4901. https://doi.org/10.1021/ma9002903.
(11) Wan, L.; Ruiz, R.; Gao, H.; Patel, K. C.; Albrecht, T. R.; Yin, J.; Kim, J.; Cao, Y.; Lin, G. The Limits of Lamellae-Forming PS- *b* -PMMA Block Copolymers for Lithography. *ACS Nano* **2015**, *9* (7), 7506–7514. https://doi.org/10.1021/acsnano.5b02613.
(12) Sinturel, C.; Bates, F. S.; Hillmyer, M. A. High χ–Low *N* Block Polymers: How Far Can We Go? *ACS Macro Lett.* **2015**, *4* (9), 1044–1050. https://doi.org/10.1021/acsmacrolett.5b00472.
(13) Pula, P.; Leniart, A.; Majewski, P. W. Solvent-Assisted Self-Assembly of Block Copolymer Thin Films. *Soft Matter* **2022**, *18* (21), 4042–4066. https://doi.org/10.1039/D2SM00439A.
(14) Xiong, S.; Li, D.; Hur, S.-M.; Craig, G. S. W.; Arges, C. G.; Qu, X.-P.; Nealey, P. F. The Solvent Distribution Effect on the Self-Assembly of Symmetric Triblock Copolymers during Solvent Vapor Annealing. *Macromolecules* **2018**, *51* (18), 7145–7151. https://doi.org/10.1021/acs.macromol.8b01275.
(15) Baruth, A.; Seo, M.; Lin, C. H.; Walster, K.; Shankar, A.; Hillmyer, M. A.; Leighton, C. Optimization of Long-Range Order in Solvent Vapor Annealed Poly(Styrene)- *Block* -Poly(Lactide) Thin Films for Nanolithography. *ACS Appl. Mater. Interfaces* **2014**, *6* (16), 13770–13781. https://doi.org/10.1021/am503199d.
(16) Jackson, E. A.; Lee, Y.; Radlauer, M. R.; Hillmyer, M. A. Well-Ordered Nanoporous ABA Copolymer Thin Films via Solvent Vapor Annealing, Homopolymer Blending, and Selective Etching of ABAC Tetrablock Terpolymers. *ACS Appl. Mater. Interfaces* **2015**, *7* (49), 27331–27339. https://doi.org/10.1021/acsami.5b08856.
(17) Choi, E.; Park, S.; Ahn, H.; Lee, M.; Bang, J.; Lee, B.; Ryu, D. Y. Substrate-Independent Lamellar Orientation in High-Molecular-Weight Polystyrene- *b* -Poly(Methyl Methacrylate) Films: Neutral Solvent Vapor and Thermal Annealing Effect. *Macromolecules* **2014**, *47* (12), 3969–3977. https://doi.org/10.1021/ma500716f.
(18) Lee, D.; Lee, J.; Park, J.; Chang, T. Orientation of Microphase in Polystyrene- *b* -Polyisoprene Thin Film under Solvent Vapor Annealing. *Macromolecules* **2020**, *53* (21), 9611–9618. https://doi.org/10.1021/acs.macromol.0c01017.
(19) Lodge, T. P.; Pan, C.; Jin, X.; Liu, Z.; Zhao, J.; Maurer, W. W.; Bates, F. S. Failure of the Dilution Approximation in Block Copolymer Solutions. *J Polym Sci B Polym Phys* **1995**, *33* (16), 2289–2293. https://doi.org/10.1002/polb.1995.090331614.
(20) Ji, S.; Liu, C.-C.; Son, J. G.; Gotrik, K.; Craig, G. S. W.; Gopalan, P.; Himpsel, F. J.; Char, K.; Nealey, P. F. Generalization of the Use of Random Copolymers To Control the Wetting Behavior of Block Copolymer Films. *Macromolecules* **2008**, *41* (23), 9098–9103. https://doi.org/10.1021/ma801861h.
(21) Pang, Y.; Wan, L.; Huang, G.; Zhang, X.; Jin, X.; Xu, P.; Liu, Y.; Han, M.; Wu, G.-P.; Ji, S. Controlling Block Copolymer–Substrate Interactions by Homopolymer Brushes/Mats. *Macromolecules* **2017**, *50* (17), 6733–6741. https://doi.org/10.1021/acs.macromol.7b00743.
(22) Ji, S.; Liu, G.; Zheng, F.; Craig, G. S. W.; Himpsel, F. J.; Nealey, P. F. Preparation of Neutral Wetting Brushes for Block Copolymer Films from Homopolymer Blends. *Advanced Materials* **2008**, *20* (16), 3054–3060. https://doi.org/10.1002/adma.200800048.
(23) She, M.-S.; Lo, T.-Y.; Ho, R.-M. Long-Range Ordering of Block Copolymer Cylinders Driven by Combining Thermal Annealing and Substrate Functionalization. *ACS Nano* **2013**, *7* (3), 2000–2011. https://doi.org/10.1021/nn305725q.
(24) Pang, Y.; Jin, X.; Huang, G.; Wan, L.; Ji, S. Directed Self-Assembly of Styrene-Methyl Acrylate Block Copolymers with Sub-7 Nm Features via Thermal Annealing. *Macromolecules* **2019**, *52* (8), 2987–2994. https://doi.org/10.1021/acs.macromol.9b00174.

(25) Wang, H. S.; Kim, K. H.; Bang, J. Thermal Approaches to Perpendicular Block Copolymer Microdomains in Thin Films: A Review and Appraisal. *Macromol. Rapid Commun.* **2019**, *40* (4), 1800728. https://doi.org/10.1002/marc.201800728.
(26) Thurn-Albrecht, T.; Steiner, R.; DeRouchey, J.; Stafford, C. M.; Huang, E.; Bal, M.; Tuominen, M.; Hawker, C. J.; Russell, T. P. Nanoscopic Templates from Oriented Block Copolymer Films. *Advanced Materials* **2000**, *12* (11), 787–791. https://doi.org/10.1002/(SICI)1521-4095(200006)12:11<787::AID-ADMA787>3.0.CO;2-1.
(27) Xu, T.; Stevens, J.; Villa, J. A.; Goldbach, J. T.; Guarini, K. W.; Black, C. T.; Hawker, C. J.; Russell, T. P. Block Copolymer Surface Reconstuction: A Reversible Route to Nanoporous Films. *Adv Funct Materials* **2003**, *13* (9), 698–702. https://doi.org/10.1002/adfm.200304374.
(28) Yin, J.; Yao, X.; Liou, J.-Y.; Sun, W.; Sun, Y.-S.; Wang, Y. Membranes with Highly Ordered Straight Nanopores by Selective Swelling of Fast Perpendicularly Aligned Block Copolymers. *ACS Nano* **2013**, *7* (11), 9961–9974. https://doi.org/10.1021/nn403847z.
(29) Vriezekolk, E. J.; de Weerd, E.; de Vos, W. M.; Nijmeijer, K. Control of Pore Size and Pore Uniformity in Films Based on Self-Assembling Block Copolymers. *Journal of Polymer Science Part B: Polymer Physics* **2014**, *52* (23), 1568–1579. https://doi.org/10.1002/polb.23600.
(30) Wei, M.; Sun, W.; Shi, X.; Wang, Z.; Wang, Y. Homoporous Membranes with Tailored Pores by Soaking Block Copolymer/Homopolymer Blends in Selective Solvents: Dissolution versus Swelling. *Macromolecules* **2016**, *49* (1), 215–223. https://doi.org/10.1021/acs.macromol.5b02133.
(31) Kennemur, J. G. Poly(Vinylpyridine) Segments in Block Copolymers: Synthesis, Self-Assembly, and Versatility. *Macromolecules* **2019**, *52* (4), 1354–1370. https://doi.org/10.1021/acs.macromol.8b01661.
(32) Doerk, G. S.; Li, R.; Fukuto, M.; Rodriguez, A.; Yager, K. G. Thickness-Dependent Ordering Kinetics in Cylindrical Block Copolymer/Homopolymer Ternary Blends. *Macromolecules* **2018**, *51* (24), 10259–10270. https://doi.org/10.1021/acs.macromol.8b01773.
(33) Jin, C.; Olsen, B. C.; Luber, E. J.; Buriak, J. M. Nanopatterning via Solvent Vapor Annealing of Block Copolymer Thin Films. *Chem. Mater.* **2017**, *29* (1), 176–188. https://doi.org/10.1021/acs.chemmater.6b02967.
(34) Hulkkonen, H.; Salminen, T.; Niemi, T. Automated Solvent Vapor Annealing with Nanometer Scale Control of Film Swelling for Block Copolymer Thin Films. *Soft Matter* **2019**, *15* (39), 7909–7917. https://doi.org/10.1039/C9SM01322A.
(35) Selkirk, A.; Prochukhan, N.; Lundy, R.; Cummins, C.; Gatensby, R.; Kilbride, R.; Parnell, A.; Baez Vasquez, J.; Morris, M.; Mokarian-Tabari, P. Optimization and Control of Large Block Copolymer Self-Assembly via Precision Solvent Vapor Annealing. *Macromolecules* **2021**, *54* (3), 1203–1215. https://doi.org/10.1021/acs.macromol.0c02543.
(36) Wu, S. Calculation of Interfacial Tension in Polymer Systems. *J. polym. sci., C Polym. symp.* **2007**, *34* (1), 19–30. https://doi.org/10.1002/polc.5070340105.
(37) Panda, A. S.; Lee, Y.-C.; Shastry, T.; Manesi, G.-M.; Avgeropoulos, A.; Ho, R.-M. Controlled Orientation of Silicon-Containing Diblock Copolymer Thin Films by Substrate Functionalization Under Vacuum. *Macromolecules* **2023**, *56* (3), 841–849. https://doi.org/10.1021/acs.macromol.2c01765.
(38) Owens, D. K.; Wendt, R. C. Estimation of the Surface Free Energy of Polymers. *J. Appl. Polym. Sci.* **1969**, *13* (8), 1741–1747. https://doi.org/10.1002/app.1969.070130815.
(39) SciAnalysis;Https://Github.Com/CFN-Softbio/SciAnalysis (Accessed November 4,2023).
(40) Russell, S. T.; Bae, S.; Subramanian, A.; Tiwale, N.; Doerk, G.; Nam, C.-Y.; Fukuto, M.; Yager, K. G. Priming Self-Assembly Pathways by Stacking Block Copolymers. *Nat Commun* **2022**, *13* (1), 6947. https://doi.org/10.1038/s41467-022-34729-0.

(41) Lee, S.; Subramanian, A.; Tiwale, N.; Kisslinger, K.; Mumtaz, M.; Shi, L.-Y.; Aissou, K.; Nam, C.-Y.; Ross, C. A. Resolving Triblock Terpolymer Morphologies by Vapor-Phase Infiltration. *Chem. Mater.* **2020**, *32* (12), 5309–5316. https://doi.org/10.1021/acs.chemmater.0c01647.
(42) Kim, E.; Ahn, H.; Park, S.; Lee, H.; Lee, M.; Lee, S.; Kim, T.; Kwak, E.-A.; Lee, J. H.; Lei, X.; Huh, J.; Bang, J.; Lee, B.; Ryu, D. Y. Directed Assembly of High Molecular Weight Block Copolymers: Highly Ordered Line Patterns of Perpendicularly Oriented Lamellae with Large Periods. *ACS Nano* **2013**, *7* (3), 1952–1960. https://doi.org/10.1021/nn3051264.
(43) Sparnacci, K.; Antonioli, D.; Perego, M.; Giammaria, T. J.; Seguini, G.; Ferrarese Lupi, F.; Zuccheri, G.; Gianotti, V.; Laus, M. High Temperature Surface Neutralization Process with Random Copolymers for Block Copolymer Self-Assembly. *Polymer International* **2017**, *66* (3), 459–467. https://doi.org/10.1002/pi.5285.
(44) Mansky, P.; Liu, Y.; Huang, E.; Russell, T. P.; Hawker, C. Controlling Polymer-Surface Interactions with Random Copolymer Brushes. *Science* **1997**, *275* (5305), 1458–1460. https://doi.org/10.1126/science.275.5305.1458.
(45) Cavicchi, K. A.; Berthiaume, K. J.; Russell, T. P. Solvent Annealing Thin Films of Poly(Isoprene-b-Lactide). *Polymer* **2005**, *46* (25), 11635–11639. https://doi.org/10.1016/j.polymer.2005.09.072.
(46) Gong, J.; Ahn, H.; Kim, E.; Lee, H.; Park, S.; Lee, M.; Lee, S.; Kim, T.; Kwak, E.-A.; Ryu, D. Y. Rapid Structural Reorganization in Thin FIlms of Block Copolymer Self-Assembly. **2012**.
(47) Berezkin, A. V.; Papadakis, C. M.; Potemkin, I. I. Vertical Domain Orientation in Cylinder-Forming Diblock Copolymer Films upon Solvent Vapor Annealing. **2016**.
(48) Larsen, M. Hansen Solubility Parameters and SWCNT Composites. In *Procedings of the 17th International Conference on Composite Materials, ICCM-17, Edinburg*; 2009.
(49) Park, S.; Wang, J.-Y.; Kim, B.; Chen, W.; Russell, T. P. Solvent-Induced Transition from Micelles in Solution to Cylindrical Microdomains in Diblock Copolymer Thin Films. *Macromolecules* **2007**, *40* (25), 9059–9063. https://doi.org/10.1021/ma071321z.
(50) Xiong, S.; Wan, L.; Ishida, Y.; Chapuis, Y.-A.; Craig, G. S. W.; Ruiz, R.; Nealey, P. F. Directed Self-Assembly of Triblock Copolymer on Chemical Patterns for Sub-10-Nm Nanofabrication *via* Solvent Annealing. *ACS Nano* **2016**, *10* (8), 7855–7865. https://doi.org/10.1021/acsnano.6b03667.
(51) *Polymer Handbook, 2 Volumes Set, 4th Edition | Wiley*. https://www.wiley.com/en-us/Polymer+Handbook%2C+2+Volumes+Set%2C+4th+Edition-p-9780471479369 (accessed 2024-01-28).
(52) Yoshida, H.; Suh, H. S.; Ramirez-Herunandez, A.; Lee, J. I.; Aida, K.; Wan, L.; Ishida, Y.; Tada, Y.; Ruiz, R.; De Pablo, J.; Nealey, P. F. Topcoat Approaches for Directed Self-Assembly of Strongly Segregating Block Copolymer Thin Films. *J. Photopol. Sci. Technol.* **2013**, *26* (1), 55–58. https://doi.org/10.2494/photopolymer.26.55.
(53) *Is There A Correlation Between Contact Angle And Stain Repellency?*. Coatings World. https://www.coatingsworld.com/issues/2016-07-01/view_features/is-there-a-correlation-between-contact-angle-and-stain-repellency/ (accessed 2024-01-28).
(54) Bai, W.; Yager, K. G.; Ross, C. A. *In Situ* Characterization of the Self-Assembly of a Polystyrene–Polydimethylsiloxane Block Copolymer during Solvent Vapor Annealing. *Macromolecules* **2015**, *48* (23), 8574–8584. https://doi.org/10.1021/acs.macromol.5b02174.
(55) Samant, S.; Strzalka, J.; Yager, K. G.; Kisslinger, K.; Grolman, D.; Basutkar, M.; Salunke, N.; Singh, G.; Berry, B.; Karim, A. Ordering Pathway of Block Copolymers under Dynamic Thermal Gradients Studied by *in Situ* GISAXS. *Macromolecules* **2016**, *49* (22), 8633–8642. https://doi.org/10.1021/acs.macromol.6b01555.
(56) Helfand, E.; Tagami, Y. Theory of the Interface between Immiscible Polymers. II. *The Journal of Chemical Physics* **1972**, *56* (7), 3592–3601. https://doi.org/10.1063/1.1677735.

(57) Song, J.-Q.; Liu, Y.-X.; Zhang, H.-D. A Surface Interaction Model for Self-Assembly of Block Copolymers under Soft Confinement. *The Journal of Chemical Physics* **2016**, *145* (21), 214902. https://doi.org/10.1063/1.4968599.
(58) Trombly, D. M.; Pryamitsyn, V.; Ganesan, V. Self-Assembly of Diblock Copolymer on Substrates Modified by Random Copolymer Brushes. *Macromolecules* **2011**, *44* (24), 9867–9881. https://doi.org/10.1021/ma202075d.
(59) Moh, L. C. H.; Losego, M. D.; Braun, P. V. Solvent Quality Effects on Scaling Behavior of Poly(Methyl Methacrylate) Brushes in the Moderate- and High-Density Regimes. *Langmuir* **2011**, *27* (7), 3698–3702. https://doi.org/10.1021/la2002139.
(60) Yamamoto, S.; Ejaz, M.; Tsujii, Y.; Fukuda, T. Surface Interaction Forces of Well-Defined, High-Density Polymer Brushes Studied by Atomic Force Microscopy. 2. Effect of Graft Density. *Macromolecules* **2000**, *33* (15), 5608–5612. https://doi.org/10.1021/ma991988o.
(61) Elmahdy, M. M.; Drechsler, A.; Uhlmann, P.; Stamm, M. Swelling and Surface Interactions of End-Grafted Poly(2-Vinylpyridine) Layers in Acidic Solution: Influence of Grafting Density and Salt Concentration. *Langmuir* **2016**, *32* (22), 5451–5459. https://doi.org/10.1021/acs.langmuir.6b00316.
(62) Han, E.; Kang, H.; Liu, C.; Nealey, P. F.; Gopalan, P. Graphoepitaxial Assembly of Symmetric Block Copolymers on Weakly Preferential Substrates. *Advanced Materials* **2010**, *22* (38), 4325–4329. https://doi.org/10.1002/adma.201001669.
(63) Durand, W. J.; Carlson, M. C.; Maher, M. J.; Blachut, G.; Santos, L. J.; Tein, S.; Ganesan, V.; Ellison, C. J.; Willson, C. G. Experimental and Modeling Study of Domain Orientation in Confined Block Copolymer Thin Films. *Macromolecules* **2016**, *49* (1), 308–316. https://doi.org/10.1021/acs.macromol.5b02262.
(64) Jeong, U.; Ryu, D. Y.; Kho, D. H.; Lee, D. H.; Kim, J. K.; Russell, T. P. Phase Behavior of Mixtures of Block Copolymer and Homopolymers in Thin Films and Bulk. **2003**, *36* (10).
(65) Doerk, G. S.; Yager, K. G. Diversifying Self-Assembled Phases in Block Copolymer Thin Films via Blending. *Phys. Rev. Materials* **2023**, *7* (12), 120301. https://doi.org/10.1103/PhysRevMaterials.7.120301.
(66) Mahmoudi, P.; Matsen, M. W. Entropic Segregation of Short Polymers to the Surface of a Polydisperse Melt. *Eur. Phys. J. E* **2017**, *40* (10), 85. https://doi.org/10.1140/epje/i2017-11575-7.
(67) Toth, K.; Bae, S.; Osuji, C. O.; Yager, K. G.; Doerk, G. S. Film Thickness and Composition Effects in Symmetric Ternary Block Copolymer/Homopolymer Blend Films: Domain Spacing and Orientation. *Macromolecules* **2021**, *54* (17), 7970–7986. https://doi.org/10.1021/acs.macromol.1c01032.
(68) Jeong, U.; Ryu, D. Y.; Kho, D. H.; Kim, J. K.; Goldbach, J. T.; Kim, D. H.; Russell, T. P. Enhancement in the Orientation of the Microdomain in Block Copolymer Thin Films upon the Addition of Homopolymer. *Advanced Materials* **2004**, *16* (6), 533–536. https://doi.org/10.1002/adma.200306113.
(69) Galy, T.; Marszewski, M.; King, S.; Yan, Y.; Tolbert, S. H.; Pilon, L. Comparing Methods for Measuring Thickness, Refractive Index, and Porosity of Mesoporous Thin Films. *Microporous and Mesoporous Materials* **2020**, *291*, 109677. https://doi.org/10.1016/j.micromeso.2019.109677.
(70) Xu, T.; Goldbach, J. T.; Misner, M. J.; Kim, S.; Gibaud, A.; Gang, O.; Ocko, B.; Guarini, K. W.; Black, C. T.; Hawker, C. J.; Russell, T. P. Scattering Study on the Selective Solvent Swelling Induced Surface Reconstruction. *Macromolecules* **2004**, *37* (8), 2972–2977. https://doi.org/10.1021/ma0355204.

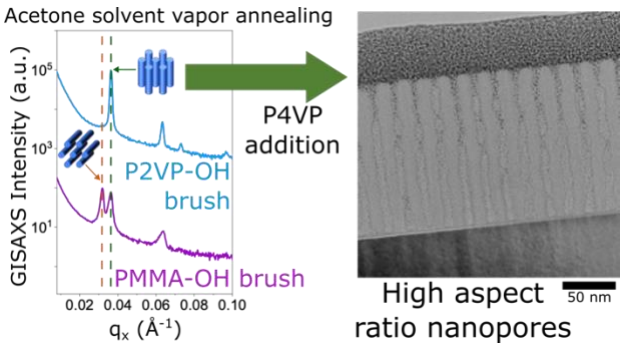
Acetone solvent vapor annealing
GISAXS Intensity (a.u.)
10^5
10^3
10^1
P2VP-OH brush
PMMA-OH brush
0.02 0.04 0.06 0.08 0.10
q_x (Å^{-1})
P4VP addition
High aspect ratio nanopores
50 nm